Check for updates

OPEN

Universal size ratios of Gaussian polymers with complex architecture: radius of gyration vs hydrodynamic radius

Khristine Haydukivska[1,4], Viktoria Blavatska[1,4] & Jarosław Paturej[2,3,4✉]

We study the impact of arm architecture of polymers with a single branch point on their structure in solvents. Many physical properties of polymer liquids strongly dependent on the size and shape measures of individual macromolecules, which in turn are determined by their topology. Here, we use combination of analytical theory, based on path integration method, and molecular dynamics simulations to study structural properties of complex Gaussian polymers containing f^c linear branches and f^r closed loops grafted to the central core. We determine size measures such as the gyration radius R_g and the hydrodynamic radii R_H, and obtain the estimates for the size ratio R_g/R_H with its dependence on the functionality $f = f^c + f^r$ of grafted polymers. In particular, we obtain the quantitative estimate of the degree of compactification of these polymers with increasing number of closed loops f^r as compared to linear or star-shape molecules of the same total molecular weight. Numerical simulations corroborate theoretical prediction that R_g/R_H decreases towards unity with increasing f. These findings provide qualitative description of polymers with complex architecture in θ solvents.

Polymer macromolecules of complex branched structure attract considerable attention both from academical[1,2] and applied[3,4] perspective, being encountered as building blocks of materials like synthetic and biological gels[5], thermoplastics[6], melts and elastomers[7,8]. High functionality of polymers provides novel properties with applications in diverse fields like drug delivery[9], tissue engineering[10], super-soft materials[11], and antibacterial surfaces[12] etc. On the other hand, multiple loop formation in macromolecules is often encountered and plays an important role in biological processes such as stabilization of globular proteins[13] or transcriptional regularization of genes[14]. In this concern, it is of fundamental interests to study conformational properties of complex polymer architectures.

In statistical description of polymers, a considerable attention is paid to the universal quantities describing equilibrium size and shape of typical conformation adapted by individual macromolecule in a solvent[15,16]. In particular, many physical properties are manifestations of the underlaying polymer conformation, including the hydrodynamic properties of polymer fluids[17], the folding dynamics and catalytic activity of proteins[18] etc. As a size measure of a single macromolecule one usually considers the mean square radius of gyration R_g^2, which is directly measurable in static scattering experiments[19,20]. Denoting coordinates of the monomers along the polymer chain by $\vec{r}_n, n = 1, \ldots, N$, this quantity is defined as:

$$\langle R_g^2 \rangle = \frac{1}{2N^2} \sum_{n,m} \langle (\vec{r}_n - \vec{r}_m)^2 \rangle, \tag{1}$$

and is thus given by a trace of gyration tensor $\mathbf{Q}$[21]. Here and below, $\langle (\ldots) \rangle$ denotes ensemble average over possible polymer conformations. Another important quantity that characterizes the size of a polymer coil is hydrodynamic

[1]Institute for Condensed Matter Physics of the National Academy of Sciences of Ukraine, 1, Svientsitskii Str., 79011 Lviv, Ukraine. [2]Institute of Physics, University of Silesia, 75 Pułku Piechoty 1, 41-500 Chorzów, Poland. [3]Leibniz Institute of Polymer Research Dresden e.V., Hohe Str. 6, 01069 Dresden, Germany. [*]These authors contributed equally: Khristine Haydukivska, Viktoria Blavatska, and Jarosław Paturej. ✉email: jaroslaw.paturej@us.edu.pl
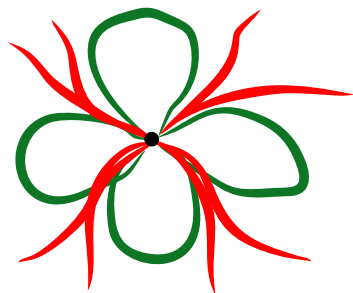
Figure 1. Schematic presentation of rosette polymer topology comprised $f^r = 4$ rings (green) and $f^c = 8$ linear chains (red) grafted to a central core (black).

radius R_H, which is directly obtained in dynamic light scattering experiments[22–24]. This quantity was introduced based on the following motivation[25]. According to the Stokes–Einstein equation, the diffusion coefficient D of a spherical particle of radius R_s in a solvent of viscosity η at temperature T is given by:

$$D = \frac{k_B T}{6\pi \eta R_s} \tag{2}$$

where k_B is Boltzmann constant. In order to generalize the above relation for the case of molecules of more complex shape, their center-of-mass diffusion coefficient D is given by Eq. (2) with R_s replaced by R_H. The latter is given as the average of the reciprocal distances between all pairs of monomers[26]:

$$\langle R_H^{-1} \rangle = \frac{1}{N^2} \sum_{n,m} \left\langle \frac{1}{|\vec{r}_n - \vec{r}_m|} \right\rangle. \tag{3}$$

Namely, R_H is related with the averaged components of the Oseen tensor $\mathbf{H}_{nm}$ characterizing the hydrodynamic interactions between monomers n and m[27]. To compare R_g^2 and R_H^{-1}, it is convenient to introduce the universal size ratio

$$\rho = \sqrt{R_g^2}/R_H, \tag{4}$$

which does not depend on any details of chemical microstructure and is governed by polymer architecture. In the present paper we restrict our consideration to the ideal (Gaussian) polymers, i.e. monomers have no excluded volume. This to a certain extent corresponds to the behavior of flexible polymers in the so-called θ-solvents. Note that our theoretical approach is not capable to correctly capture structural properties of more rigid branched polymers like dendrimers or molecular bottlebrushes. The intrinsic rigidity of these macromolecules is controlled by steric repulsions between connected branches or grafts. This approach allows to obtain the exact analytical results for the set of universal quantities characterizing conformational properties of macromolecules. In particular, for a linear Gaussian polymer chain the exact analytical result for the ratio (4) in $d = 3$ dimensions reads[28–30]:

$$\rho_{\text{chain}} = \frac{8}{3\sqrt{\pi}} \approx 1.5045. \tag{5}$$

The universal ratio of a Gaussian ring polymer was calculated in Refs. [29,31,32] and is given by

$$\rho_{\text{ring}} = \frac{\sqrt{2\pi}}{2} \approx 1.2533. \tag{6}$$

The validity of theoretically derived ratios ρ_{chain} and ρ_{ring} was confirmed in several simulation studies [30,32,33].

The distinct example of branched macromolecule is the so-called rosette polymer[34], containing f^c linear chains and f^r closed loops (rings), radiating from the same branching point (see Fig. 1). Note that for $f^r = 0$ one restores architecture of a star polymer with f^c functionalized linear chains radiating from a central core, for which an exact analytical result is known for the size ratio (Ref.[26]):

$$\rho_{\text{star}} = \frac{8\sqrt{f(3f^c - 2)}}{3(f^c)^2 \sqrt{\pi}} (\sqrt{2} - 1)(\sqrt{2} + f^c). \tag{7}$$

The estimates for ρ_{star} have been also obtained by numerical Monte-Carlo simulations[35]. Using molecular dynamics (MD) simulations, Uehara and Deguchi derived the universal size ratios for macromolecules such as single ring ($f^c = 0$, $f^r = 1$), tadpole ($f^r = 1$, $f^c = 1$) and double ring ($f^r = 2$, $f^c = 0$)[32]. The overview of existing literature data for universal size ratios obtained in analytical ρ_{theory} and numerical ρ_{sim} investigations are listed in Table 1. Note large discrepancy between previous numerical study of star polymers[35] and the theoretical result of Eq. (7). This significant difference between theory and simulations is due to too short chains that were used in Ref. [35] with maximum degree of polymerization $N = 150$. As it will be shown the finite-size effect of polymer

Topology	f^c	f^r	ρ_{theory}	ρ_{sim}
Chain	1	0	1.5045 Eq. (5)	1.5045 ± 0.0005[33]
Ring	0	1	1.253 Eq. (6)	1.253 ± 0.013[32]
Star	3	0	1.40 Eq. (7)	1.11[35]
Star	4	0	1.33 Eq. (7)	1.04[35]
Tadpol	1	1	1.415 Eq. (29)	1.380 ± 0.021[32]
Double ring	0	2	1.217 Eq. (30)	1.215 ± 0.011[32]

Table 1. Literature data for the universal size ratio for different polymer topologies, derived using analytical theory ρ_{theory} and numerical simulations ρ_{sim}. The theoretical values for tadpol and double ring architectures were calculated on the basis of our general analytical result, cf. Eq. (28).

chains strongly affects measured value of ρ. In our numerical study we calculate ρ in the asymptotic limit. For this purpose we simulated long polymer chains with degree of polymerization equal to $N = 6400$.

The aim of the present work is to extend the previous analysis of rosette-like polymers[34], by thoroughly studying their universal size characteristics. For this purpose we apply the analytical theory, based on path-integration method, and extensive numerical molecular dynamics simulations. The layout of the paper is as follows. In the next section, we introduce the continuous chain model and provide the details of analytical calculation of the universal size ratios ρ for various polymer architectures applying path integration method. In Sect. 3 we describe the numerical model and details of MD simulations. In the same section we present numerical results and compare them with our theoretical predictions. We draw conclusions and remarks in Sect. 4.

Analytical approach

The model. Within the frame of continuous chain model[36], a single Gaussian polymer chain of length L is represented as a path $\vec{r}(s)$, parameterized by $0 < s < L$. We adapt this model to more complicated branched polymer topologies, containing in general f^c linear branches and f^r closed rings (see Fig. 1). In the following, let us use notation $f = f^c + f^r$ for total functionality of such structure. The weight of each ith path ($i = 1, \ldots, f$) is given by

$$W_i = e^{-\frac{1}{2}\int_0^L ds \left(\frac{d\vec{r}_i}{ds}\right)^2}. \tag{8}$$

The corresponding partition function of rosette polymer is thus:

$$Z_{f^c f^r} = \frac{\int \mathcal{D}\{\vec{r}\} \prod_{j=1}^{f^r} \delta(\vec{r}_j(L) - \vec{r}_j(0)) \prod_{i=1}^{f} \delta(\vec{r}_i(0)) \, W_i}{\int \mathcal{D}\{\vec{r}\} \prod_{i=1}^{f} \delta(\vec{r}_i(0)) \, W_i}, \tag{9}$$

where $\mathcal{D}\{\vec{r}\}$ denotes multiple path integration over trajectories $\vec{r}_i(s)$ ($i = 1, \ldots, f$) assumed to be of equal length $L_i = L$, the first product of δ-functions reflects the fact that all $f^c + f^r$ trajectories start at the same point (central core), and the second δ-functions product up to f^r describes the closed ring structures of f^r trajectories (their starting and end points coincide). Note that (9) is normalised in such a way that the partition function of the system consisting of $f^c + f^r$ open linear Gaussian chains (star-like structure) is unity. The expression for partition function of rosette-like polymer architecture have been evaluated in Ref. [34] and in Gaussian approximation reads:

$$Z_{f^c f^r} = (2\pi L)^{-df^r/2}. \tag{10}$$

where d denotes spatial dimensionality. Within the frame of presented model, the expression for mean square gyration radius from Eq. (1) can be rewritten as

$$\langle R_g^2 \rangle = \frac{1}{2(fL)^2} \sum_{i,j=1}^{f} \int_0^L \int_0^L ds_2 \, ds_1 \langle (\vec{r}_i(s_2) - \vec{r}_j(s_1))^2 \rangle, \tag{11}$$

whereas the expression (3) for hydrodynamic radius reads:

$$\langle R_H^{-1} \rangle = \frac{1}{(fL)^2} \sum_{i,j=1}^{f} \int_0^L \int_0^L ds_2 \, ds_1 \langle |\vec{r}_i(s_2) - \vec{r}_j(s_1)|^{-1} \rangle, \tag{12}$$

where $\langle (\ldots) \rangle$ denotes averaging over an ensemble of all possible configurations defined as:
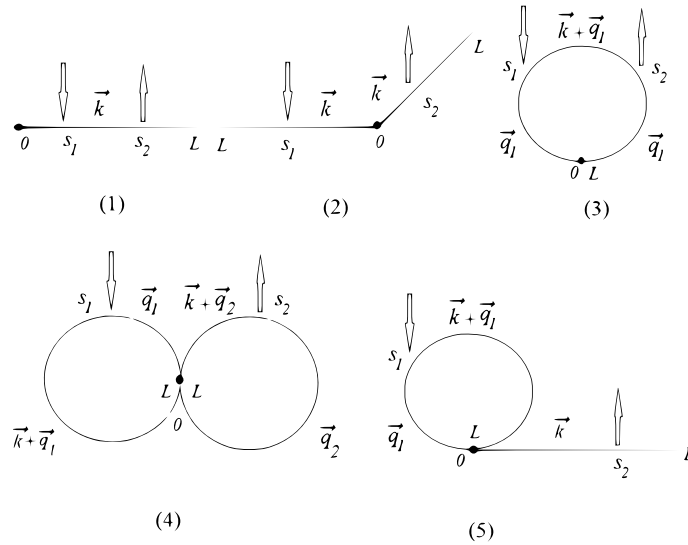
Figure 2. Diagrammatic presentation of contributions into $\langle R_H^{-1} \rangle$ according to (12). Solid lines are schematic presentation of polymer paths, arrows denote point s_1, s_2.

$$\langle(\ldots)\rangle = \frac{1}{Z_{f_c,f_r}}$$

$$\times \frac{\int \mathcal{D}\{\vec{r}\} \prod_{j=1}^{f^r} \delta(\vec{r}_j(L)-\vec{r}_j(0)) \prod_{i=1}^{f} \delta(\vec{r}_i(0))(\ldots) W_i}{\int \mathcal{D}\{\vec{r}\} \prod_{i=1}^{f} \delta(\vec{r}_i(0)) \, W_i}. \tag{13}$$

Calculation of hydrodynamic radius and universal size ratio. The crucial point in the calculation of the hydrodynamic radius is utilization of the following equality[37]:

$$|\vec{r}|^{-1} = (2\pi)^{-d} \int d\vec{k} \, 2^{d-1} \pi^{\frac{d-1}{2}} \Gamma\left(\frac{d-1}{2}\right) k^{1-d} e^{i\vec{r}\vec{k}}. \tag{14}$$

where $\Gamma(x)$ is Gamma function. Applying the above expression to Eq. (12) allows to rewrite the mean reciprocal distance from the definition of R_H as

$$\langle|\vec{r}_i(s_2) - \vec{r}_j(s_1)|^{-1}\rangle = (2\pi)^{-d} \int d\vec{k} \, 2^{d-1} \pi^{\frac{d-1}{2}} \times$$
$$\times \Gamma\left(\frac{d-1}{2}\right) k^{1-d} \langle \xi(s_1, s_2) \rangle \tag{15}$$

with notation

$$\xi(s_1, s_2) \equiv e^{i\vec{k}(\vec{r}_i(s_2)-\vec{r}_j(s_1))}. \tag{16}$$

Below we will apply path integration approach to calculate the mean reciprocal distances.

Exploiting the Fourier-transform of the δ-functions in definition (13)

$$\delta(\vec{r}_j(L) - \vec{r}_j(0)) = (2\pi)^{-d} \int d\vec{q}_j \, e^{-i\vec{q}_j(\vec{r}_j(L)-\vec{r}_j(0))} \tag{17}$$

we get a set of wave vectors $\vec{q}_j$ with $j = 1, \ldots, f^r$ associated with f^r closed loop trajectories, which is an important point in following evaluation. To visualize different contributions into $\langle|\vec{r}_i(s_2) - \vec{r}_j(s_1)|^{-1}\rangle$, it is convenient to use the diagrammatic technique (see Fig. 2). Taking into account the general rules of diagram calculations[15], each segment between any two restriction points s_a and s_b is oriented and bears a wave vector $\vec{p}_{ab}$ given by a sum of incoming and outcoming wave vectors injected at restriction points and end points. At these points, the flow of wave vectors is conserved. A factor $\exp\left(-p_{ab}^2(s_b - s_a)/2\right)$ is associated with each segment. An integration is to be made over all independent segment areas and over wave vectors injected at the end points.

To make these rules more clear, let us start with diagram (1), corresponding to the case when both points s_1 and s_2 are located along any linear arm of rosette polymer. The vector $\vec{k}$ is injected at restriction point s_1 and

the segment $s_2 - s_1$ is associated with factor $\exp\left(-k^2(s_2-s_1)/2\right)$. Next step is performing integration over k. Passing to d-dimensional spherical coordinates, we have:

$$\int \mathrm{d}\vec{k}\, k^{1-d} f(k^2) = \frac{2\pi^{d/2}}{\Gamma\left(\frac{d}{2}\right)} \int \mathrm{dk}\, f(k^2),$$

(18)

and thus integration over k can be easily performed

$$\int_0^\infty \mathrm{dk}\, e^{-\frac{k^2(s_2-s_1)}{2}} = \sqrt{\frac{\pi}{2}} (s_2 - s_1)^{-1/2}.$$

(19)

The analytic expression corresponding to contribution from diagram (1) thus reads

$$\langle \xi(s_1, s_2)\rangle_{(1)} = \frac{(2\pi^{d+1})^{\frac{1}{2}}}{\Gamma\left(\frac{d}{2}\right)} \int_0^L \mathrm{ds}_2 \int_0^{s_2} \mathrm{ds}_1 (s_2-s_1)^{-\frac{1}{2}}.$$

(20)

Diagram (2) describes the situation when restriction points s_1 and s_2 are located along two different linear arms of rosette polymer. We thus have a segment of length $(s_2 + s_1)$ between them, associated with factor $\exp\left(-k^2(s_2+s_1)/2\right)$. After performing integration over k we receive

$$\langle \xi(s_1, s_2)\rangle_{(2)} = \frac{(2\pi^{d+1})^{\frac{1}{2}}}{\Gamma\left(\frac{d}{2}\right)} \int_0^L \mathrm{ds}_2 \int_0^L \mathrm{ds}_1 (s_2+s_1)^{-\frac{1}{2}}.$$

(21)

In the case (3), both s_1 and s_2 are located on the closed loop, let it be the loop with $j = 1$. Here, we need to take into account the wave vector $\vec{q}_1$, "circulating" along this loop, so that three segments should be taken into account with lengths s_1, $s_2 - s_1$, and $L - s_2$, correspondingly, with associated factors $\exp\left(-q_1^2 s_1/2\right)$, $\exp\left(-(q_1 + k)^2(s_2 - s_1)/2\right)$, $\exp\left(-q^2(L - s_2)/2\right)$. Integration over the wave vector q_1 gives

$$(2\pi)^{-d} \int \mathrm{d}\vec{q}_1\, e^{-\frac{q_1^2 L}{2} - \vec{q}\vec{k}(s_2-s_1)} =$$

$$= (2\pi L)^{-d/2} (s_2 - s_1)^{-\frac{1}{2}} e^{\frac{k^2(s_2-s_1)^2}{2L}}.$$

(22)

After performing final integration over k we receive

$$\langle \xi(s_1, s_2)\rangle_{(3)} = \frac{(2\pi^{d+1})^{\frac{1}{2}}}{\Gamma\left(\frac{d}{2}\right)} \int_0^L ds_2 \int_0^{s_2} ds_1$$

$$\times \left(s_2 - s_1 - \frac{(s_2-s_1)^2}{L}\right)^{-\frac{1}{2}}.$$

(23)

Following the same scheme, we receive analytic expressions, corresponding to diagrams (4) and (5) on Fig. 2:

$$\langle \xi(s_1, s_2)\rangle_{(4)} = \frac{(2\pi^{d+1})^{\frac{1}{2}}}{\Gamma\left(\frac{d}{2}\right)} \int_0^L ds_2 \int_0^L ds_1$$

$$\times \left(s_2 + s_1 - \frac{s_2^2}{L} - \frac{s_1^2}{L}\right)^{-\frac{1}{2}},$$

(24)

$$\langle \xi(s_1, s_2)\rangle_{(5)} = \frac{(2\pi^{d+1})^{\frac{1}{2}}}{\Gamma\left(\frac{d}{2}\right)} \int_0^L ds_2 \int_0^L ds_1$$

$$\times \left(s_2 + s_1 - \frac{s_1^2}{L}\right)^{-\frac{1}{2}}.$$

(25)

Note that each diagram in Fig. 2 is associated with the corresponding combinatorial factor. Namely, the contribution (1) in above expressions is taken with the pre-factor f^c, contribution (2) with $\frac{f^c(f^c-1)}{2}$, (3) with f^r, (4) with $\frac{f^r(f^r-1)}{2}$ and the last contribution (5) with the pre-factor $f^r f^c$. Summing up all contributions from Eq. (25) with taking into account corresponding pre-factors, on the base of Eq. (15) we finally obtain the expression for the hydrodynamic radius of a rosette structure:

$$
\begin{aligned}
\langle R_{h,\text{rosette}} \rangle = {} & \frac{\Gamma\left(\frac{d-1}{2}\right)}{\Gamma\left(\frac{d}{2}\right)\sqrt{2}} 12(f^c + f^r)^2\sqrt{L} \\
& \times \left[-6f_r\pi\left(\sqrt{2}(f^r-1) - 2f^r + 1\right) \right. \\
& + 16\left(\sqrt{2}-1\right)f^c\left(\sqrt{2}+f^c\right) \\
& \left. + 3f^cf^r\left(10\arcsin\left(\frac{\sqrt{5}}{5}\right) - \pi + 4\right) \right]^{-1}.
\end{aligned}
\tag{26}
$$

The expression for the mean square gyration radius of a rosette architecture is[34]:

$$
\begin{aligned}
\langle R^2_{g,\text{rosette}} \rangle = {} & \frac{Ld}{12(f^r+f^c)^2}[f^r(2f^r-1) \\
& + 2f^c(3f^c-2) + 8f^rf^c].
\end{aligned}
\tag{27}
$$

Finally, using Eqs. (26) and (27), we calculate the the universal size ratio (4) of rosette-like polymer architecture in Gaussian approximation:

$$
\begin{aligned}
\rho_{\text{rosette}} = {} & \frac{\sqrt{6d}\,\Gamma\left(\frac{d-1}{2}\right)}{72(f^r+f^c)^3\Gamma\left(\frac{d}{2}\right)} \\
& \times \sqrt{6(f^c)^2 + 8f^cf^r + 2(f^r)^2 - 4f^c - f^r} \\
& \times \left[-6f_r\pi\left(\sqrt{2}(f^r-1) - 2f^r + 1\right) \right. \\
& + 16\left(\sqrt{2}-1\right)f^c\left(\sqrt{2}+f^c\right) \\
& \left. + 3f^cf^r\left(10\arcsin\left(\frac{\sqrt{5}}{5}\right) - \pi + 4\right) \right].
\end{aligned}
\tag{28}
$$

Substituting $d = 3$ in expression (28), for $f^r = 0$, both at $f^c = 1$ and $f^c = 2$ we restore the universal size ratio of a linear polymer (5), whereas $f^c > 2$ and $f^r = 0$ gives the expression for a star polymer (7). For $f^c = 0$ and $f^r = 1$ we reproduce the known analytical expression of a single ring from Eq. (6). Consequently $f^c = 0$ and $f^r = 2$ Eq. (28) provides the formula for universal size ratio of a star comprised of two ring polymers:

$$
\rho_{\text{double ring}} = \frac{\sqrt{3\pi}}{4}(3 - \sqrt{2}) \approx 1.217.
\tag{29}
$$

For $f^c = 1$ and $f^r = 1$ we find analytic expression for the so-called tadpole architecture:

$$
\begin{aligned}
\rho_{\text{tadpole}} = {} & \frac{\sqrt{22}}{96\sqrt{\pi}}\left[3\pi + 28 + 30\arcsin\left(\frac{\sqrt{5}}{5}\right)\right] \\
& \approx 1.415.
\end{aligned}
\tag{30}
$$

In Fig. 3 we plot calculated theoretical values of the universal size ratio vs number of functionalized chains for stars comprised of linear polymers with $f^c > 0$, $f^r = 0$ (red symbols) and ring polymers $f^r > 0$, $f^c = 0$ (blue) as well as rosette polymers with equal number of grafted linear chains and rings $f^r = f^c > 0$ (purple). For all architectures we observe decrease in ρ with increasing functionality. In the next subsection we compare our theoretical predictions with the result of MD simulations.

Numerical approach

The method. Numerical data in this work have been obtained from MD simulations. We consider simple three-dimensional numerical model of a rosette polymer consisting of arms which are f^c linear chains and/or f^r ring polymers. Each arm is composed of N sizeless particles of equal mass m connected by bonds. We study ideal (Gaussian) conformations of rosette polymers corresponding to a certain extent to the conformations of real rosette polymers at dilute θ solvent conditions. In our numerical model the connectivity along the polymer chain backbone is assured via harmonic potential

$$
V(r) = \frac{k}{2}(r - r_0)^2,
\tag{31}
$$

where $k = 200\,k_BT/b^2$ is the interaction strength measured in units of thermal energy k_BT and the equilibrium bond distance $r_0 = b$.
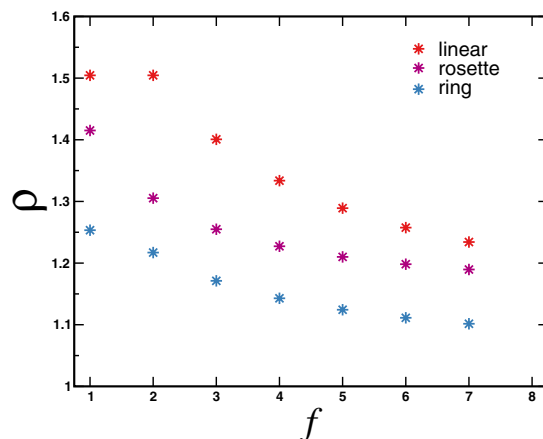
Figure 3. Summary of theoretical results for universal size ratio ρ as given by (28) vs functionality $f = f^c + f^r$ for different polymer topologies. Data for architectures containing: only linear chains (star-like polymer with $f^r = 0$) as function of $f = f^c$ (red symbols), only ring polymer (with $f^c = 0$) as function of $f = f^r$ (blue symbols) and "symmetric" rosette structure with equal number of rings and linear branches $f = f^r + f^c$ (purple symbols).
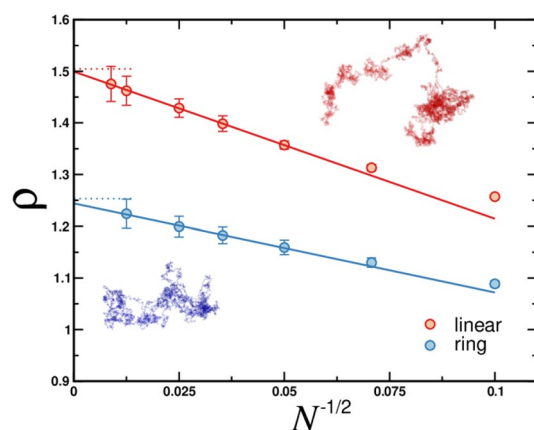

Figure 4. Molecular dynamics data for the universal size ratio ρ of linear chains (red symbols) and ring polymers (blue symbols) plotted as a function of correction-to-scaling variable $N^{-1/2}$ with corresponding simulation snapshots for polymer architectures with degree of polymerization $N = 6400$. Solid lines represent fitting functions of the general form given in Eq. (33). Horizontal dotted lines correspond to asymptotic values ρ_∞ predicted by theory, cf. Eqs. (5) and (6).

The molecular dynamics simulations were performed by solving the Langevin equation of motion for the position $\vec{r}_i = [x_i, y_i, z_i]$ of each monomer,

$$m\ddot{\vec{r}}_i = \vec{F}_i - \zeta\dot{\vec{r}}_i + \vec{F}_i^R, \quad i = 1, \ldots, fN, \tag{32}$$

which describes the motion of bonded monomers. Forces $\vec{F}_i$ in Eq. (32) above are obtained from the harmonic interaction potential between (Eq. 31). The second and third term on the right hand side of Eq. (32) is a slowly evolving viscous force $-\zeta\dot{\vec{r}}_i$ and a rapidly fluctuating stochastic force $\vec{F}_i^R$ respectively. This random force $\vec{F}_i^R$ is related to the friction coefficient ζ by the fluctuation-dissipation theorem $\langle \vec{F}_i^R(t)\vec{F}_j^R(t') \rangle = k_B T \zeta \delta_{ij} \delta(t - t')$. The friction coefficient used in simulations was $\zeta = 0.5\, m\tau^{-1}$ where $\tau = [mb^2/(k_B T)]^{1/2}$ is the unit of time. A Langevin thermostat was used to keep the temperature constant. The integration step employed to solve the equations of motions was taken to be $\Delta t = 0.0025\tau$. All simulations were performed in a cubic box with periodic boundary conditions imposed in all spatial dimensions. We used Large-scale Atomic/Molecular Massively Parallel Simulator (LAMMPS)[38] to perform simulations. Simulation snapshots were rendered using Visual Molecular Dynamics (VMD)[39].
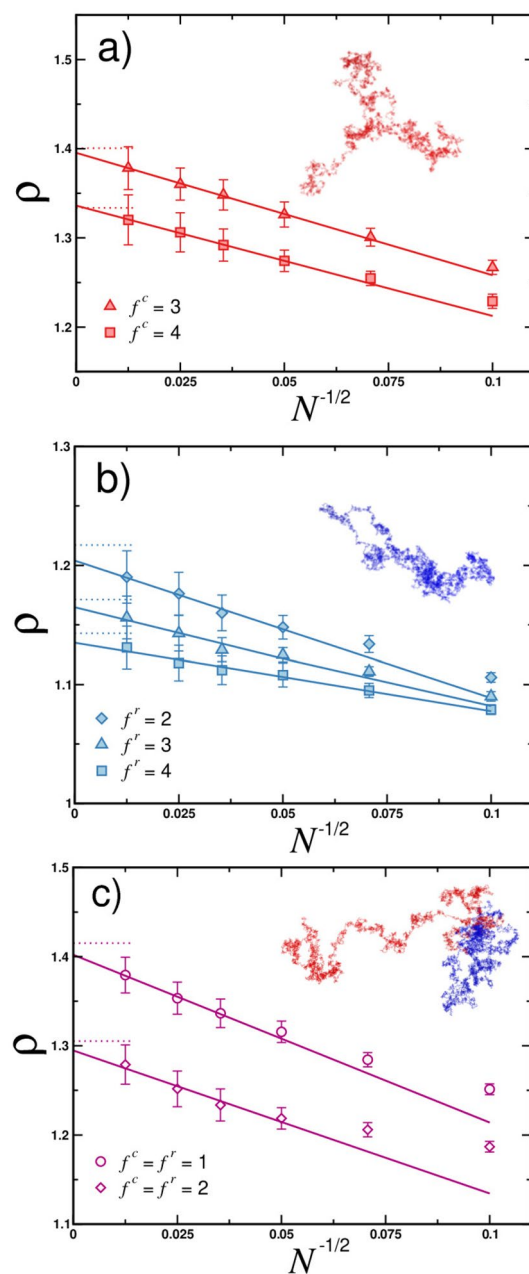
Figure 5. Molecular dynamics data for the universal size ratio ρ of star polymers comprised of a) linear, b) ring polymers and c) rosette polymers plotted as a function of correction-to-scaling variable $N^{-1/2}$. Data displayed for different amount of arms f^c and f^r as indicated. For rosette polymers data are for symmetric number of arms $f^c = f^r$. Solid lines represent fitting functions according to Eq. (33). Horizontal dotted lines correspond to asymptotic values obtained from analytical theory, see Table 2. Insets show simulation snapshots for with $N = 6400$ and: (**a**) $f^c = 3$, (**b**) $f^r = 2$ and (**c**) $f^c = f^r = 1$.

Results. Simulations of rosette polymers were performed for the following number of monomer beads per arm $N = 100, 200, 400, 800, 1600$ and 6400. The number of arms for star polymers composed of solely linear chains (i.e. with $f^r = 0$) and ring polymers (i.e. with $f^c = 0$) were varied in the range between 1 to 4. In the case of rosette polymers which are hybrid polymer architectures comprised of linear chains and ring polymers we considered two arm functionalities with $f^c = f^r = 1$ and 2. To increase conformational sampling each simulation was carried out with 50 identical molecules in a simulation box. In the course of simulations the universal size ratio was measured, cf. Eq. (4). In the numerical calculation of quantities like ρ a crucial aspect is finite degree of polymerization N that we are dealing with in simulations, while theoretically obtained values of ρ hold in the asymptotic limit $N \to \infty$. Thus, the finite-size effects (or corrections to scaling) should be appropriately taken into account. For the size ratio of an ideal linear chain, this correction is given by

f^c	f^r	ρ_{theory}	ρ_{sim}
1	0	1.504	1.499 ± 0.005
2	0	1.504	1.499 ± 0.005
3	1	1.401	1.395 ± 0.006
4	0	1.334	1.336 ± 0.006
0	1	1.253	1.244 ± 0.004
0	2	1.217	1.204 ± 0.010
0	3	1.171	1.165 ± 0.011
0	4	1.143	1.135 ± 0.012
1	1	1.415	1.401 ± 0.008
2	2	1.305	1.295 ± 0.018

Table 2. Summary of theoretical results for the size ratio ρ_{theory} calculated using Eq. (28) and asymptotic values ρ_{sim} obtained from MD simulations for rosette polymer architectures comprised of different number of f^c linear chains and f^r ring polymers.

$$\rho = \rho_\infty(1 + aN^{-\Delta}), \qquad (33)$$

where ρ_∞ is the asymptotic value obtained at $N \to \infty$, a is non-universal amplitude, Δ is the correction-to-scaling exponent for θ-solvent is $\Delta = 1/2$[30] whereas for good solvent conditions is $\simeq 0.53$[33]. In our numerical analysis we use Eq. (33) to obtain the universal size ratio in the asymptotic limit for all considered architectures. For this purpose we plot ρ vs correction-to-scaling term $N^{-1/2}$ and get $\rho = \rho_\infty$ for $N \to \infty$.

In Fig. 4 we display the results of our MD simulations for two "benchmark" systems which are Gaussian linear chain (red circles) and Gaussian ring (blue circles). For both architectures systematic increase in the size ratio is observed with increasing value of N. In the asymptotic limit $N \to \infty$ we obtain $\rho_{\text{chain}} = 1.499 \pm 0.005$ and $\rho_{\text{ring}} = 1.244 \pm 0.004$. These numerical values with very good accuracy reproduce known theoretical results. The latter are given by Eq. (5) for linear chains and by (6) for rings. The complete list of numerically derived universal size ratios and their comparison to theoretical values can be found in Table 2.

In Fig. 5 we show numerically derived universal size ratios as a function of $N^{-1/2}$ for more complex architectures. We investigated conformations of stars comprised of linear chains, stars of ring polymers and rosette polymers with equal number of grafted linear and ring chains. For all architectures we observe systematic approaching to asymptotic values predicted by theory with increasing value of N per arm. For stars of linear chains with functionality $f^c = 3$ and 4 (cf. Fig. 5a) simulations provide the following universal size ratios: 1.395 ± 0.006 and 1.336 ± 0.006. Both values are with very good agreement to the theoretical prediction given by Eq. (7). Note that the values of ρ calculated in the course of our simulations are much closer to the analytical theory results as compared to existing numerical data[35]. For stars comprised of cyclic macromolecules (cf. Fig. 5b) we reproduce the theoretical value of Eq. (29) for double ring architecture ($f^r = 2$) as well as for stars with larger number of grafted rings, cf. Eq. (28) with $f^c = 0$ and $f^r = 3$ or 4. Namely, we get 1.204 ± 0.010 for $f^r = 2$, 1.165 ± 0.011 for $f^r = 3$ and 1.135 ± 0.012 for $f^r = 4$. For the tadpole architecture, the simplest rosette polymer which is comprised of $f^c = 1$ and $f^r = 1$ arms (see snapshot in Fig. 5c), we obtain the size ratio of 1.401 ± 0.008 which matches theoretically predicted value for this type of polymer from Eq. (30). For rosette polymers with $f^c = 2$ and $f^r = 2$ our simulations provide 1.295 ± 0.018 which is comparable with the corresponding value calculated from the formula given in Eq. (28). The full list of calculated values of ρ is in Table 2.

Conclusions

We have studied by combination of analytical theory and molecular dynamics simulations conformational properties of rosette polymers which are complex macromolecules consisting of f^c linear chains (branches) and f^r closed loops (rings) radiating from the central branching point. Our focus was on characterizing structure of ideal polymer conformation with no excluded volume interactions. For this purpose we investigated basic structural quantities such as the mean square radius of gyration R_g^2, the hydrodynamic radius R_H^{-1} and most importantly the universal size ratio $\rho \equiv \sqrt{R_g^2}/R_H$. Our calculations demonstrated gradual decrease in ρ with increasing functionality $f = f^c + f^r$ of grafted polymers. The analytical results are in perfect agreement with our numerical simulations data. Since both quantities R_g^2 and R_H are directly accessible via correspondingly static and dynamic scattering techniques we hope that our results will stimulate further experimental studies on the behavior of complex polymer architectures in solutions.

References

1. Schäfer, L., von Ferber, C., Lehr, U. & Duplantier, B. Renormalization of polymer networks and stars. *Nucl. Phys. B* **374**, 473 (1992).
2. von Ferber, C. & Holovatch, Y. Copolymer networks and stars: Scaling exponents. *Phys. Rev. E* **56**, 6370 (1997).
3. Gao, C. & Yan, D. Hyperbranched polymers: From synthesis to applications. *Prog. Polym. Sci.* **29**, 183 (2004).
4. Jeon, I.-Y., Noh, H. J. & Baek, J. B. Hyperbranched macromolecules: From synthesis to applications. *Molecules* **23**, 657 (2018).

5. Djabourov, M., Nishinari, K. & Ross-Murphy, S. B. *Physical Gels from Biological and Synthetic Polymers* (Cambridge University Press, Cambridge, 2013).
6. Zhang, J., Scheiderman, D. K., Li, T., Hillmyer, M. A. & Bates, F. S. Design of graft block polymer thermoplastics. *Macromolecules* **49**, 9108 (2016).
7. Paturej, J. & Kreer, T. Hierarchical excluded volume screening in solutions of bottlebrush polymers. *Soft Matter.* **13**, 8534 (2017).
8. Paturej, J., Sheiko, S., Panyukov, S. & Rubinstein, M. Molecular structure of bottlebrush polymers in melts. *Sci. Adv.* **2**, e1601478 (2016).
9. Li, J. & Mooney, D. J. Designing hydrogels for controlled drug delivery. *Nat. Rev. Mater.* **1**, 16071 (2016).
10. Lee, K. Y. & Mooney, D. J. Hydrogels for tissue engineering. *Chem. Rev.* **101**, 1869 (2001).
11. Daniel, W. *et al.* Solvent-free, supersoft and superelastic bottlebrush melts and networks. *Nat. Mater.* **15**, 183 (2016).
12. Zhou, Y., Huang, W., Liu, J., Zhu, X. & Yan, D. Self-assembly of hyperbranched polymers and its biomedical applications. *Adv. Mater.* **22**, 4567 (2010).
13. Nagi, A. D. & Regan, L. An inverse correlation between loop length and stability in a four-helix-bundle protein. *Fold. Des.* **2**, 67 (1997).
14. Towles, K. B., Beausang, J. F., Garcia, H. G., Phillips, R. & Nelson, P. C. First-principles calculation of DNA looping in tethered particle experiments. *Phys. Biol.* **6**, 025001 (2009).
15. Des Cloizeaux, J. & Jannink, G. *Polymers in Solution: Their Modeling and Structure* (Clarendon Press, Oxford, 1990).
16. de Gennes, P. G. *Scaling Concepts in Polymer Physics* (Cornell University Press, Ithaca, 1979).
17. de la Torre, G., Llorca, O., Carrascosa, J. L. & Valpuesta, J. M. HYDROMIC: Prediction of hydrodynamic properties of rigid macromolecular structures obtained from electron microscopy images. *Eur. Biophys. J.* **30**, 457 (2001).
18. Quyang, Z. & Liang, J. Predicting protein folding rates from geometric contact and amino acid sequence. *Protein Sci.* **17**, 1256 (2008).
19. Ferri, F., Greco, M. & Rocco, M. On the determination of the average molecular weight, radius of gyration, and mass/length ratio of polydisperse solutions of polymerizing rod-like macromolecular monomers by multi-angle static light scattering. *Macromol. Symp.* **162**, 23 (2000).
20. Smilgies, D.-M. & Folta-Stogniew, E. Molecular weight-gyration radius relation of globular proteins: A comparison of light scattering, small-angle X-ray scattering and structure-based data. *J. Appl. Crystallogr.* **48**, 1604 (2015).
21. Aronovitz, J. A. & Nelson, D. R. Universal features of polymer shapes. *J. Phys.* **47**, 1445 (1986).
22. Schmidt, M. & Burchard, W. Translational diffusion and hydrodynamic radius of unperturbed flexible chains. *Macromolecules* **14**, 210 (1981).
23. Varma, B. K., Fujita, Y., Takahashi, M. & Nose, T. Hydrodynamic radius and intrinsic viscosity of polystyrene in the crossover region from θ to good-solvent conditions. *J. Polym. Sci. Polym. Phys. Ed.* **22**, 1781 (1984).
24. Linegar, K. L., Adeniran, A. E., Kostko, A. F. & Anisimov, M. A. Hydrodynamic radius of polyethylene glycol in solution obtained by dynamic light scattering. *Colloid J.* **72**, 279 (2010).
25. Doi, M. & Edwards, S. F. *The Theory of Polymer Dynamics* (Oxford University Press, Oxford, 1988).
26. Teraoka, I. *Polymer Solutions: An Introduction to Physical Properties* (John Wiley & Sons Inc, New York, 2002).
27. Kirkwood, J. G. The general theory of irreversible processes in solutions of macromolecules. *J. Polym. Sci.* **12**, 1 (1953).
28. Zimm, B. H. & Stockmayer, W. H. J. The dimensions of chain molecules containing branches and rings. *J. Chem. Phys.* **17**, 1301 (1949).
29. Burchard, W. & Schmidt, M. Static and dynamic structure factors calculated for flexible ring macromolecules. *Polymer* **21**, 745 (1980).
30. Dünweg, B., Reith, D., Steinhauser, M. & Kremer, K. Corrections to scaling in the hydrodynamic properties of dilute polymer solutions. *J. Chem. Phys.* **117**, 914 (2002).
31. Fukatsu, M. & Kurata, M. J. Hydrodynamic properties of flexible-ring macromolecules. *J. Chem. Phys.* **44**, 4539 (1966).
32. Uehara, E. & Deguchi, T. Statistical and hydrodynamic properties of topological polymers for various graphs showing enhanced short-range correlation. *J. Chem. Phys.* **145**, 164905 (2016).
33. Clisby, N. & Dünweg, B. High-precision estimate of the hydrodynamic radius for self-avoiding walks. *Phys. Rev. E* **94**, 052102 (2016).
34. Blavatska, V. & Metzler, R. Conformational properties of complex polymers: Rosette versus star-like structures. *J. Phys. A: Math. Theor.* **48**, 135001 (2015).
35. Shida, K., Ohno, K., Kawazoe, M. Y. & Nakamura, Y. Hydrodynamic factors for linear and star polymers on lattice under the theta condition. *Polymer* **45**, 1729 (2004).
36. Edwards, S. F. The statistical mechanics of polymers with excluded volume. *Proc. Phys. Soc. Lond.* **85**, 613 (1965).
37. Haydukivska, K. & Blavatska, V. Ring polymers in crowded environment: Conformational properties. *J. Chem. Phys.* **141**, 094906 (2014).
38. Plimpton, S.J. Fast Parallel Algorithms for Short-Range Molecular Dynamics. *J. Comp. Phys.* **117**, 1 (1995). (http://lammps.sandia.gov)
39. Humphrey, W., Dalke, A. & Schulten, K. V. M. D. Visual molecular dynamics. *J. Mol. Graphics* **14**, 33 (1996).

Acknowledgements

Author contributions

All authors designed the research and wrote the manuscript. K.H. and V.B. provided theoretical predictions. J.P. performed computer simulations.

Competing interests

The authors declare no competing interests.

Additional information

Correspondence and requests for materials should be addressed to J.P.

Reprints and permissions information is available at www.nature.com/reprints.

Publisher's note Springer Nature remains neutral with regard to jurisdictional claims in published maps and institutional affiliations.